# Methodology to derive well-calibrated thermometers: a new glass-composition geothermometer for olivine-bearing glassy samples at one atmospher

Alessandro Fabbrizio, Václav Špillar

Institute of Petrology and Structural Geology, Faculty of Science, Charles University, Prague, Czech Republic

## Abstract

This work describes the methodology used to develop a new glass-composition geothermometer by multiple linear least-squares regression analysis of experimental data available in literature. The geothermometer is applicable to natural olivine-bearing glassy samples quenched at one atmosphere. The calibration data set includes a total of 543 anhydrous experiments performed at one atmosphere which produced olivine coexisting with glass ($\pm$ other phases). The accuracy of the geothermometer has been verified using an independent set of randomly selected one atmosphere anhydrous experimental samples external to the calibration data set. The new proposed equation reads: $T(°C) = 1054.1\pm6.5 + (1458.0\pm23.5)(X_{MgO})^{liq} - (267.1\pm45.8)(X_{CaO})^{liq} + (116.3\pm30.9)(X_{Na2O} + X_{K2O})^{liq}$, where the terms such as $(X_{MgO})^{liq}$ represent the cation fraction of MgO in the liquid. The new geothermometer is able to reproduce the calibration temperatures within a standard error of estimate (SEE) of $\pm23°$ C and to predict the temperatures for the test data set with a SEE of $\pm25°$ C. The proposed equation, when compared to previous models, gives the lowest systematic error. Moreover, we mathematically demonstrate that the comparison of the slope and the intercept parameters of the regression line against the 1:1 line leads to correct evaluation of the model only when a regression of observed or measured (in the $y$-axis as dependent variable) *vs*. predicted or calculated (in the $x$-axis as independent variable) is used.

Keywords: olivine-glass geothermometer; linear regression; calibration; test data; equation; temperature; model.

## 1. Introduction

In volcanology it is often important to determine the temperature ($T$) at which lava flows erupt and lava lakes cool down. Such information is crucial for understanding lava rheology and crystallization history, as well as for monitoring present day and for studying past volcanic eruptions [e.g., Costa el al., 2013; de Maisonneuve et al., 2012, 2013; Oeser et al., 2018]. A geothermometer based on a regression analysis of experimental data (i.e., calibration data), to be useful, should give the lowest systematic error when used to

predict $T$ for other experimental data not used in the regression (i.e., test data). In the ideal case, slope and intercept of the regression line of the measured or observed (in the $y$-axis) *vs.* calculated or predicted (in the $x$-axis) temperatures should be one and zero, respectively. Given that the slope and intercept parameters define a linear relationship between the measured and calculated temperatures, they can be used to test how far the model is from the ideal line 1:1, therefore, how much the model suffers for the systematic error. In the absence of testing of the regression model, the calculated temperatures may be affected by gross systematic error and in turn be meaningless.

In this study, we describe the general methodology that should be followed in deriving the regression equations for geothermometers. We then employ this approach and formulate a new geothermometer based on anhydrous liquid composition in equilibrium with olivine $\pm$ other phases at one atmosphere. In order to test the ability of a new formulation to recover the $T$ from olivine-saturated one atmosphere anhydrous experiments, we compare the new model with previous glass-composition geothermometers. Moreover, we noticed that the evaluation of the model by comparison of the slope and the intercept of the regression line against the 1:1 line depends on which variable (predicted or observed data) is treated as dependent or independent variable. A short review of some previous work shows that there is no consensus on it, given that plots of predicted (in the $y$-axis) *vs.* observed (in the $x$-axis) are commonly used as well as plots of observed (in the $y$-axis) *vs.* predicted (in the $x$-axis) to estimate the slope and intercept. From a mathematical point of view, we show that only the slope and the intercept values estimated by plotting the observed (in the $y$-axis, dependent variable) *vs.* predicted (in the $x$-axis, independent variable) is correct and should be used to provide an appropriate interpretation of the model performance.

## 2. Geothermometers based on glass composition in equilibrium with olivine

Despite the fact that basaltic compositions are predominant among volcanic rocks only few geothermometers applicable to liquids in equilibrium with olivine ($\pm$ other phases) have been proposed in the last 30 years [Helz and Thornber, 1987; Beattie, 1993; Montierth et al., 1995; Putirka, 2008]. The simplest models relate $T$ to the concentration (wt%) of MgO in a liquid ($MgO^{liq}$), and were calibrated using the experimental data obtained at 1-atm with specific bulk compositions [Helz and Thornber, 1987; Montierth et al., 1995]. The thermometer of Helz and Thornber [1987]:

$$T\,(°C) = 20.1 MgO^{liq} + 1014°\,C \tag{1}$$

was experimentally-calibrated explicitly for Kilauean lavas using basaltic and picritic Kilauean starting compositions. This geothermometer was calibrated over a temperature range of 1060° C to 1260° C, giving an uncertainty associated with the calculated temperatures of $\pm10°$ C, with the purpose to constrain the quench temperature of the drill core samples recovered from the Kilauea Iki lava lake. It has also been used to monitor changes in the lava temperature both at the vent [Helz et al., 1991] and during its transport within the lava tube system [Helz, 1993; Cashman et al., 1994], and to analyze the thermal histories of recent eruptions at Kilauea [Helz et al., 1995].

Subsequently, Montierth et al. [1995] developed another empirical glass-composition-based geothermometer with the aim to obtain the quench temperature of any glassy Mauna Loa sample with an uncertainty of $\pm10°$ C:

$$T\,(°C) = 23.0 MgO^{liq} + 1012°\,C \tag{2}$$

This equation was calibrated in the temperature range of 1110 to 1310° C using specific Mauna Loa compositions, which are slightly different with respect to those of Kilauea, being richer in $SiO_2$ and poorer in $TiO_2$, FeO, $K_2O$, and $P_2O_5$ for comparable MgO contents [Montierth et al., 1995].

These experimental calibrations (eq. 1 and 2) were developed for the specific bulk compositions and with the aim to obtain the quench temperatures solely for the lavas from the Kilauea and Mauna Loa volcanoes.

Beattie [1993] developed a useful empirical thermometer solely based on the constraint that the activity-composition relationships in the melt phases should allow equilibration temperatures to be calculated as accurately as possible. The combination of these activity models yields the following equation:

$$T \,(°C) = [13603 + 4943 \times 10^{-7}(P \times 10^9 - 10^5)]/[6.26 + 2\ln D^{ol/liq}{}_{Mg} +$$

$$2\ln(1.5(C^L{}_{NM})) + 2\ln(3(C^L{}_{SiO2})) - NF] - 273.15, \tag{3}$$

where $P$ is a pressure in GPa, $D^{ol/liq}{}_{Mg} = (0.666 - (-0.049(X_{MnO})^{liq} + 0.027(X_{FeO})^{liq}))/((X_{MgO})^{liq} + 0.259(X_{MnO})^{liq} + 0.0299(X_{FeO})^{liq})$, $(C^L{}_{NM}) = (X_{FeO})^{liq} + (X_{MnO})^{liq} + (X_{MgO})^{liq} + (X_{CaO})^{liq} + (X_{CoO})^{liq} + (X_{NiO})^{liq}$, $(C^L{}_{SiO2}) = (X_{SiO2})^{liq}$, $NF = 3.5\ln(1 - (X_{AlO1.5})^{liq}) + 7\ln(1 - (X_{TiO2})^{liq})$, and the terms such as $(X_{MnO})^{liq}$ represent the cation fractions of MnO in the liquid. When predicting temperature for 1302 anhydrous olivine-saturated experimental data, the eq. (3) captures 94% of the experimental temperature variations with a standard error of estimate (SEE) of $\pm 44°$ C [Putirka, 2008].

Later, to expand the applicability range of the early thermometers of Helz and Thornber [1987] and Montierth et al. [1995], Putirka [2008] developed other models calibrated on a database of 1536 olivine-saturated experimental data. The simple linear correlation between the temperature and MgO content (wt%) in the liquid becomes:

$$T \,(°C) = 26.3 MgO^{liq} + 994.4° \text{ C} \tag{4}$$

giving the SEE of $\pm 71°$ C and capturing 84% of the experimental temperature variations. Other empirical expressions considering additional compositional terms and the effect of pressure were developed with the aim to further reduce the error [Putirka, 2008]:

$$T \,(°C) = 754 + 190.6(Mg\#^{liq}) + 25.52(MgO^{liq}) + 9.585(FeO^{liq}) + 14.87(Na_2O +$$

$$K_2O)^{liq} - 9.176(H_2O^{liq}), \tag{5}$$

and

$$T \,(°C) = 815.3 + 265.5(Mg\#^{liq}) + 15.37(MgO^{liq}) + 8.61(FeO^{liq}) + 6.646(Na_2O$$

$$+ K_2O)^{liq} - 12.83(H_2O^{liq}) + 39.16P, \tag{6}$$

where $Mg\#^{liq}$ is a molar ratio calculated as $Mg\#^{liq} = (MgO^{liq}/40.3)/(MgO^{liq}/40.3 + FeO^{liq}/71.85)$, $P$ is a pressure in GPa and the remaining terms are weight percentages of oxides in the liquid. The equations (5) and (6) give a SEE of $\pm 51°$ C and $\pm 60°$ C, respectively.

The addition of different compositional parameters including water and of a pressure term have reduced the overall accuracy of the thermometer, when compared to the early works of Helz and Thornber [1987] and Montierth et al. [1995], but have greatly expanded its applicability. The equations (4-6) are applicable to any volcanic rocks saturated at least with olivine over wider range of conditions: $P$ up to 14.4 GPa, $T$ = 729-2000° C, SiO$_2$ = 31.5-73.64 wt%, sum of alkalis (Na$_2$O + K$_2$O) up to 14.3 wt%, H$_2$O up to 18.6 wt%. However, the equations (4-6) have not been tested for their ability to predict $T$ for the experimental data not used for the calibration. It is thus unclear to what extent these equations can be used to calculate reliable temperatures for natural samples.

Another thermometer developed by Yang et al. [1999] and updated by Putirka [2008] places further constraints on the compositional degrees of freedom requiring the liquid being in equilibrium exclusively with olivine, plagioclase and clinopyroxene:

$$T \,(°C) = -583 + 3141(X_{SiO2})^{liq} + 15779(X_{Al2O3})^{liq} + 1338.6(X_{MgO})^{liq} -$$

$$31440((X_{SiO2})^{liq}(X_{Al2O3})^{liq}) + 77.67P, \tag{7}$$

where the terms such as $(X_{SiO2})^{liq}$ represent the mole fraction of SiO$_2$ in the liquid and $P$ is the pressure in GPa. This equation is able to reproduce the temperature for the calibration data set (73 experimental data) with a SEE of $\pm 19°$ C and $R^2$ of 0.92, and those for 119 test data with a SEE = $\pm 26°$ C and $R^2$ of 0.75.

The aim of this work is to define and elucidate the methodology of work that should be followed in order to calibrate and test new empirically derived thermometric equations. We achieve this task by presenting a new glass-

composition geothermometer based on olivine-bearing anhydrous glasses synthesized at 1-atm that would be applicable to shallow magmatic systems, to determine and track the changes in temperature of olivine-bearing samples from pillow lavas, lava flows, and lava lakes.

# 3. Methods

## 3.1 Calibration range and component calculation procedure

The new model is based on a regression analysis of 1-atm and olivine-saturated ($\pm$ other phases) anhydrous experiments performed using both natural and synthetic compositions (supplementary material). Experiments that crystallized olivine at 1-atm but performed by using model compositions lacking one or more main chemical compounds were not included in the database. The reason for this choice is that a model composition lacking $TiO_2$, FeO or alkalis, etc., cannot be considered fully representative of a natural composition. Consequently, the result of the regression could be biased by these compositions if they represent a large fraction of the database. The selected experiments cover the temperature and compositional range of 1021-1530° C, $37.1 \leq SiO_2 \leq 72.4$ wt% and $0 \leq Na_2O + K_2O \leq 14.3$ wt%, respectively. The liquid compositions (wt%), with iron oxide considered as all FeO, are recalculated as cation fractions following this procedure: first, the weight percentage of each oxide is divided by its molecular weight having only one cation (i.e., 60.08 for $SiO_2$, 50.98 for $AlO_{1.5}$). Then, these cation proportions are converted to cation fractions by normalizing each oxide by the sum of the cation proportions [Putirka, 2008]. Original oxide percentages, not renormalized to 100 wt%, were used for calculating the cation fractions. It should be noted that the use of un-normalized or normalized analyses to 100 wt% gives the same result when the analyses are expressed as cation fractions.

## 3.2 Data and regression strategies

A total of 701 experimental data were collected from the literature and 20% of them, 140 data, were randomly chosen as a reserve to be used as a test data for the thermometer. Multiple linear least-squares regression analysis was applied to the calibration data set ($n = 561$) and the experiments that yielded $T$ estimates outside of a 2σ standard error of estimate (SEE) for the calibration data ($n = 18$) were considered suspect and excluded from the model. Then, the remaining 543 experimental temperatures of the calibration data set, without the outliers, were regressed once again to obtain the final equation.

Basaltic compositions are the most representative for both calibration and test data, followed by basaltic andesite and andesite (Figure 1). Also, these compositions represent about 2/3 of both databases and the remaining 1/3 is represented by foidite, trachybasalt, basanite, trachyandesite, basaltic trachyandesite, phonotephrite, tephriphonolite, picrobasalt, trachyte, phonolite, rhyolite and dacite; in order of decreasing abundance. The most represented temperatures are those in the range of 1100-1250° C corresponding to about 75% of the experimental data for both calibration and test data sets (Figure 1). The temperatures in the range of 1000-1100° C represent 14% of the experimental data in the calibration data set and 9% of those in the test data set, whereas 12% of the calibration data and 16% of the test data represent temperatures above 1250° C (Figure 1). In this sense, we consider the test data set to be representative of the calibration data set in term of compositional variation and temperature range.

For creating the model and to avoid over-fitting of the data the t-ratios (calculated as the ratios between the coefficients and their standard errors and thus representing a measure of the precision with which the regression coefficients are measured; e.g., Rawlings et al. [1998]) were checked for all variables, looking for the t-ratios $\geqslant 5$, and the F-ratio (a measure of how the overall result of the regression is statistically significant; e.g., Rawlings et al. [1998]) was checked in order to achieve the maximum value similarly to the approach used in Putirka et al. [2003]. Next, the chosen variables were checked using partial-regression leverage plots to understand their importance in the calibration of the model. Finally, when several models had been calibrated, they were compared based on their ability to predict temperatures for the test data set. We looked for the model having the lowest standard error of estimate (SEE) on temperature, and whose regression slope and intercept for measured *vs.* calculated temperatures most closely approached to one and zero, respectively. Finally, the model errors were compared to the experimental temperatures and liquid compositions in order to exclude their mutual correlation.
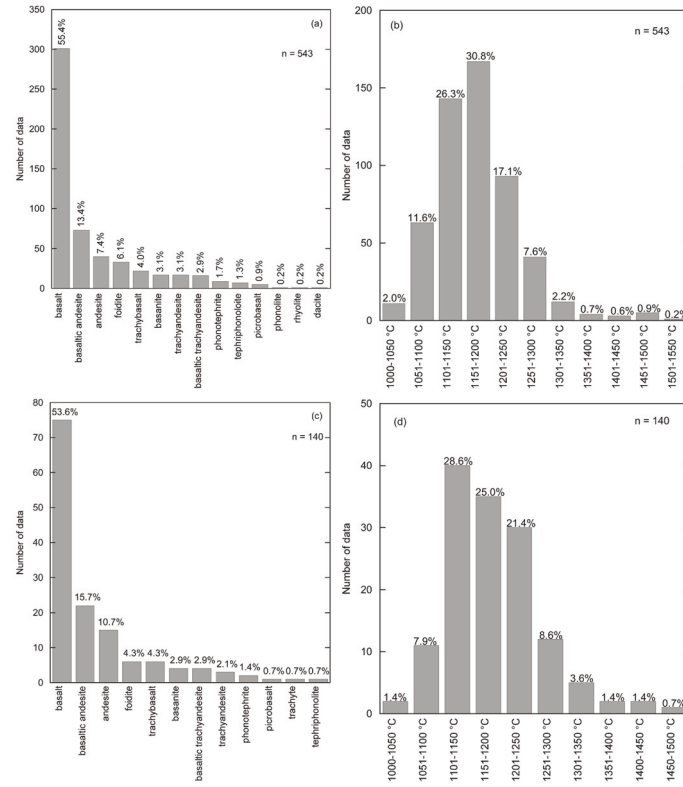
**Figure 1.** Number of samples for the calibration (a, b) and test data set (c, d) as a function of rock composition (a, c) and experimental temperature (b, d).

# 4. Results

Result of the regression is a new glass-composition thermometer applicable only to olivine-bearing glassy rocks, having the following empirical expression:

$$T\,(°C) = 1054.1 \pm 6.5 + (1458.0 \pm 23.5)(X_{MgO})^{liq} - (267.11 \pm 45.8)(X_{CaO})^{liq} +$$

$$(116.3 \pm 30.9)(X_{Na2O} + X_{K2O})^{liq}, \tag{8}$$

where the terms such as $(X_{MgO})^{liq}$ represent the cation fraction of MgO in the liquid. The equation (8) yields SEE of $\pm 23$ and $\pm 25°$ C for calibration and test data, respectively, with corresponding $R^2$ values of 0.91 and 0.90. The equation (8) shows the lowest systematic error; the addition of other compositional terms does not improve the result of the regression significantly.

The slope ($m$) and the intercept ($c$) of measured $vs.$ calculated temperatures closely approach the ideal values of one and zero, respectively, for the calibration data set (i.e., $m = 1$ and $c = 4 \times 10^{-10°}$ C), whereas the regression line for the test data has a slope of 0.99 and an intercept of $+12.4°$ C. Given the strict adherence of both regression lines to the ideal 1:1 line, the equation (8) describes both data sets with high precision (Figure 2). The regression line for the calibration data is nearly coincident with the ideal 1:1 line, whereas the regression line of the test data approaches the ideal line with an uncertainty of less than $\pm 1°$ C in the temperature range of 1100-1250° C, it overestimates the temperature by 1.8° C at 1000° C, whereas it underestimates the temperature by 3.5° C at 1500° C. Furthermore, the residuals of the test data are uncorrelated with $T$ and with all individual liquid compositional parameters, indicating that there is no systematic error, that no variables are missing in the model, and that the model residuals represent random errors.
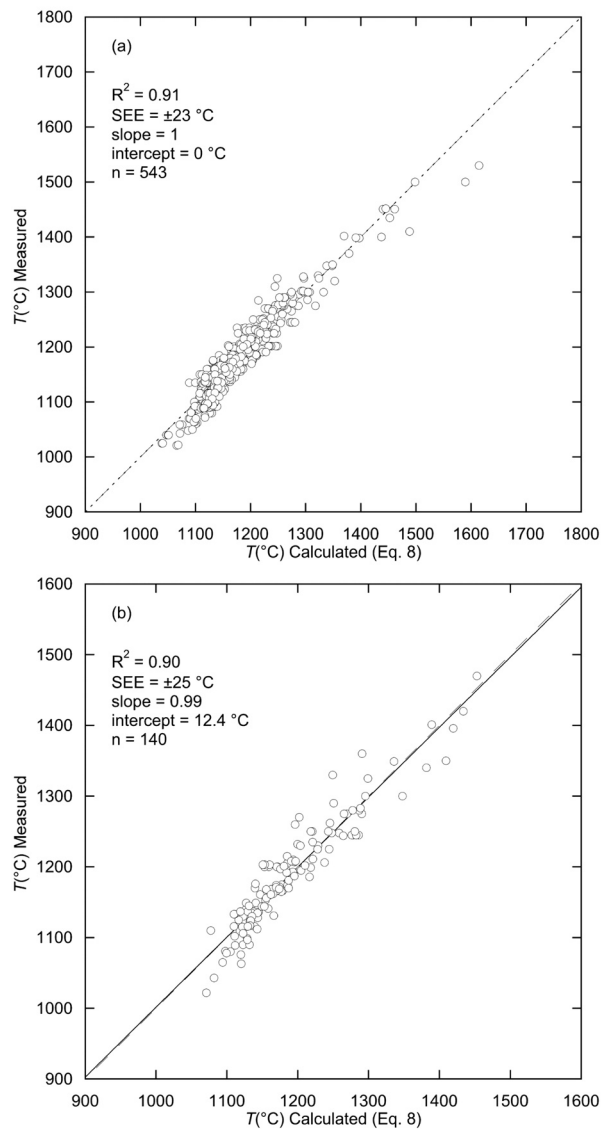
**Figure 2.** Calculated and measured temperatures are compared for the proposed new glass geothermometer using both the calibration (a) and the test (b) data sets. In panel (a) the regression line is nearly coincident with the 1:1 line. In panel (b) the solid line is the regression line and the dashed line is the 1:1 line. Calibration data are for the liquids saturated with olivine ± other phases taken from: Arndt [1977]; Baker and Eggler [1987]; Baker et al., [1994]; Barclay and Carmichael [2004]; Barr et al., [2009]; Bartels et al., [1991]; Bender et al., [1978]; Chen et al., [1982]; Delano [1977]; Dunn and Sen [1994]; Elkins et al., [2003]; Fram and Longhi [1992]; Gee and Sack [1988]; Grove and Beaty [1980]; Grove and Bryan [1983]; Grove et al., [1982, 1992, 2003]; Grove and Juster [1989]; Herd et al., [2009]; Ishibashi and Sato [2007]; Jurewicz et al., [1993]; Juster et al., [1989]; Kennedy et al., [1990]; Kinzler and Grove [1985]; Longhi and Pan [1988]; Longhi et al., [1978]; Mahood and Baker [1986]; Matzen et al., [2011, 2013, 2017]; McCoy and Lofgren [1999]; Medard et al., [2004]; Medard and Grove [2008]; Meen [1987, 1990]; Monders et al., [2007]; Parman et al., [1997]; Prissel et al., [2016]; Sack et al., [1987]; Scoates et al., [2006]; Stamper et al., [2014]; Stolper [1977]; Thy et al., [1998, 2006]; Tormey et al., [1987]; Vander Auwera and Longhi [1994]; Vander Auwera et al., [1998]; Veksler et al., [2007]; Wang and Gaetani [2008]; Zhang et al., [2018]. Test data are also the liquids saturated with olivine ± other phases and are taken from: Arndt [1977]; Baker et al., [1994]; Barr et al., [2009]; Bender et al., [1978]; Delano [1977]; Dunn and Sen [1994]; Gee and Sack [1988]; Grove and Bryan [1983]; Grove et al., [1982, 1992]; Grove and Juster [1989]; Herd et al., [2009]; Ishibashi and Sato [2007]; Jurewicz et al., [1993]; Juster et al., [1989]; Kennedy et al., [1990]; Kinzler and Grove [1985]; Longhi and Pan [1988]; Longhi et al., [1978]; Mahood and Baker [1986]; Matzen et al., [2011]; McCoy and Lofgren [1989]; Meen [1987, 1990]; Parman et al., [1997]; Prissel et al., [2016]; Sack et al., [1987]; Stamper et al., [2014]; Stolper [1977]; Thy et al., [1998, 2006]; Tormey et al., [1987]; Vander Auwera and Longhi [1994]; Veksler et al., [2007]; Wang and Gaetani [2008]; Zhang et al., [2018].

# 5. Discussion

## 5.1 How to evaluate a thermometer?

As with any model fitted to the measured data a thermometer needs a criterion to evaluate its performance. For this purpose, the calculated or predicted temperatures, $T$(calculated), are plotted against the measured or observed values, $T$(measured); ideally to define a linear trend with zero intercept, $c$, and unitary slope, $m$. Despite the fact that the order in which these two variables are assigned to the independent and dependent variables, respectively (i.e., the $x$ and $y$ axes), generally matters, it is used interchangeably in many studies [e.g., cf. Putirka et al., 1996, 2003]. While the coefficient of determination, $R^2$, remains unchanged, slope and intercept of the linear trend vary for the two possible types of projections [e.g., Piñeiro et al., 2008]. As illustrated in Table 1 for the thermometer of Helz and Thornber [1987] and for our proposed eq. (8)., the choice of an independent variable makes an important difference, which can produce both false positive and false negative impressions about the fit performance.

| Thermometer | $R^2$ | Calculated as independent | | Measured as independent | |
|:---:|:---:|:---:|:---:|:---:|:---:|
| | | $m_1$ | $c_1$ (°C) | $m_2$ | $c_2$ (°C) |
| H&T[a], eq. 1 | 0.89 | 0.90 | 135 | 0.98 | 0.26 |
| This study, eq. 8 | 0.90 | 0.99 | 12.4 | 0.91 | 113 |

[a]Helz and Thornber, [1987]. Equation numbers are referenced to this study. Variables: $R^2$ – coefficient of determination; $m_1$, $c_1$ – slope and the intercept of the fitted line taking $T$(calculated) as independent variable (eq. 10a); $m_2$, $c_2$ – slope and the intercept of the fitted line taking $T$(measured) as independent variable (eq. 10b). Note that $R^2$ is identical for both types of the fit. Calculations performed for the test dataset.

**Table 1.** Comparison of calculated vs. measured and vice versa linear fits for selected thermometers.

In general, for any thermometer the measured temperature can be decomposed to a sum of the calculated temperature predicted by the thermometer and an error, $\varepsilon$:

$$T\text{(measured)} = T\text{(calculated)} + \varepsilon. \tag{9}$$

The error in the eq. (9) encompasses the measured vs. calculated differences not only due to the temperature measurement error, but also due to other effects related to physical inability of the fitting expression to describe all variations of temperature with respect to intensive parameters.

Let us now explore the two possible linear relationships for the fit of measured vs. calculated temperatures. These two fits differ in the choice of the independent variable:

$$\hat{T}\text{(measured)} = m_1 \times T\text{(calculated)} + c_1, \tag{10a}$$

$$\hat{T}\text{(calculated)} = m_2 \times T\text{(measured)} + c_2, \tag{10b}$$

where $\hat{T}$ is a temperature estimated by the linear fit and the $m_1$, $m_2$ are the slope and the $c_1$, $c_2$ are the intercept coefficients. These coefficients are related to the variance and covariance of the measured and calculated data [e.g., Kenney and Keeping, 1962]. Specifically, the slope coefficient equals to the ratio of the covariance of both measured and calculated temperature data sets to the variance of the temperature used as an independent variable (i.e., the one usually plotted on the $x$ axis). For the two possible choices of the independent variable (eq. 10a and 10b) the expressions for the slope coefficients read [e.g., Kenney and Keeping, 1962]:

$$m_1 = \frac{\text{cov}(T(\text{calculated}),T(\text{measured}))}{\text{var}(T(\text{calculated}))} \, , \tag{11a}$$

$$m_2 = \frac{\text{cov}(T(\text{calculated}),T(\text{measured}))}{\text{var}(T(\text{measured}))} \, , \tag{11b}$$

where the functions $\text{cov}(\cdot,\cdot)$ and $\text{var}(\cdot)$ are the covariance and variance, respectively, and the eq. (11a) and (11b) differ in their denominator. The relationship between measured and calculated temperatures, eq. (9), can be inserted into both expressions for the slope coefficient, eq. (11), in order to eliminate $T(\text{measured})$ from the equations. Assuming the model for $T(\text{calculated})$ is unbiased, that is, the mean value of the error $\varepsilon$ approaches zero, and after a bit of algebra we arrive to:

$$m_1 = \frac{\text{cov}(T(\text{calculated}),\varepsilon)}{\text{var}(T(\text{calculated}))} \, , \tag{12a}$$

$$m_2 = \frac{\text{var}(T(\text{calculated}) + \text{cov}(T(\text{calculated}),\varepsilon)}{\text{var}(T(\text{calculated}))+2\text{cov}(T(\text{calculated}, \varepsilon)) + \text{var}(\varepsilon)} \, . \tag{12b}$$

In the eq. (12a) for the slope coefficient $m_1$ the calculated temperature is considered to be an independent variable, whereas in the eq. (12b) for the slope coefficient $m_2$ it is the measured temperature. Let us now assume an ideal unbiased model for the $T(\text{calculated})$. In such model, the error $\varepsilon$ is a random variable which is uncorrelated to the temperature itself; in the opposite case the model would not be ideal as it could be modified to remove its residual temperature dependence. Therefore, the covariance between the calculated temperature and the error $\varepsilon$ approaches zero. The slope $m_1$, as defined by the eq. (12a), thus approaches unity. The error $\varepsilon$ itself, while it averages out to zero mean, has some nonzero and positive variance. The slope $m_2$ (eq. 12b) is thus always less than unity.

In the ideal model, the measured and calculated variables are expected to fit to a line with a unit slope. This condition is generically fulfilled only by the slope $m_1$. Therefore, if the unit slope and zero intercept of the fit of calculated $vs.$ measured data are taken as a benchmark for the model performance, then the only statistically correct way is to use the calculated temperature as an independent variable (usually on the $x$ axis). Also, this result is intuitively correct since in the simple linear regression used to perform the fitting, only the dependent variable (usually the on the $y$ axis) is assumed to be burden with an error, that is, $T(\text{measured})$ deviates by an error from the $T(\text{calculated})$. We employ the approach in which the calculated temperature is treated as an independent variable in the following section in order to compare the performance of individual thermometers.

## 5.2 Evaluation and comparison of previous olivine-saturated liquid thermometers

The calibration and the test datasets were also used to recover temperatures, $T$, for the models of Helz and Thornber [1987], Beattie [1993], Montierth et al. [1995] and Putirka [2008]; see Table 2 for comparison of the individual models. The model of Helz and Thornber [1987], i.e., the eq. (1), captures 89% of the experimental $T$ variation ($R^2 = 0.89$) with a SEE of $\pm 33°$ C. A similar result is obtained when eq. (1) is applied to the test data set ($R^2 = 0.89$, SEE $= \pm 35°$ C). However, in both cases slopes and intercepts of the regression lines of $T(\text{measured})$ $vs.$ $T(\text{calculated})$ ($y$ $vs.$ $x$) are very poor being 0.91 and 121° C for the calibration and 0.90 and 135° C for the test data sets, respectively (Figure 3).

The model of Montierth et al. [1995], i.e., the eq. (2), gives a similar estimate of $T$, with $R^2 = 0.89$ and SEE $= \pm 30°$ C when using the calibration data and $R^2 = 0.89$ and SEE $= \pm 33°$ C when using the test data. However, it is affected by higher systematic error given the slopes and the intercepts are all worse with 0.80 and 240° C for the regression line of the calibration data, and 0.79 and 252° C for the test data, respectively (Figure 3).

The model of Beattie [1993], i.e., the eq. (3), gives the best results with SEE $= \pm 21°$ C and $R^2 = 0.92$ for the calibration data, and SEE $= \pm 24°$ C and $R^2 = 0.91$ for the test data. It is also affected by high systematic errors, but at lower level compared to the other models, given the slope and intercepts of the regression lines are 0.95 and 56° C for the calibration data, and 0.94 and 77° C for the test data (Figure 3).
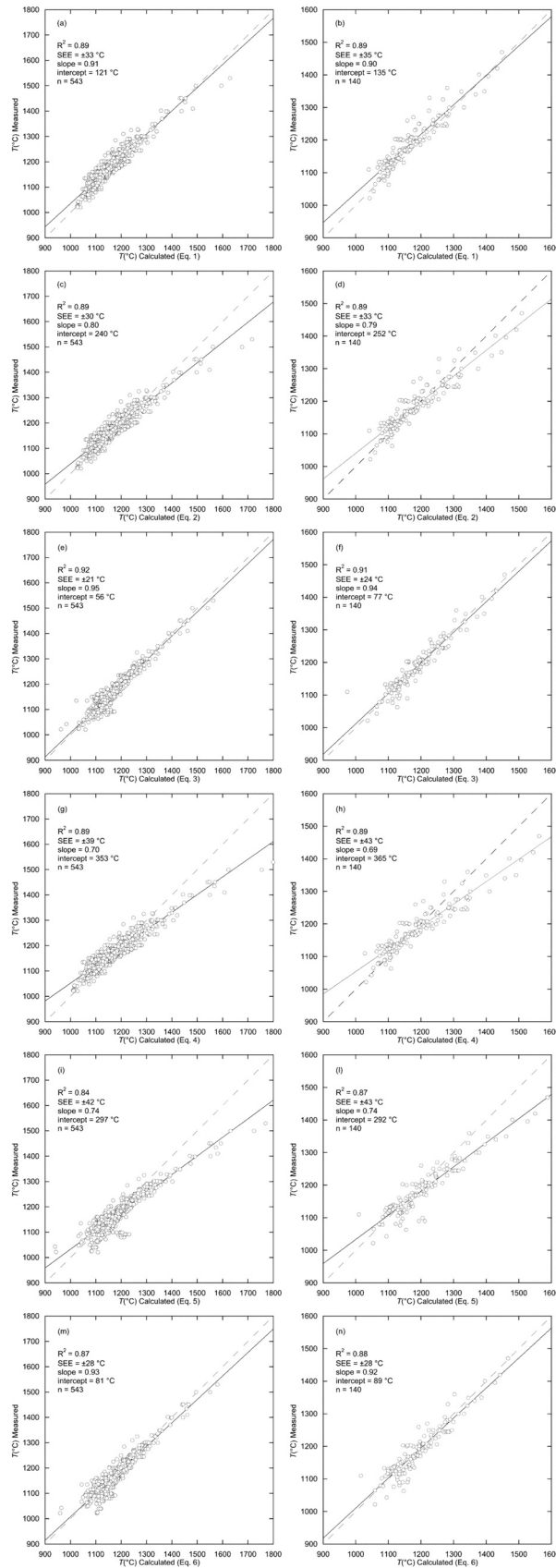
**Figure 3.** Calculated and measured temperatures are compared for the available glass geothermometers using both our calibration (a, c, e, g, i, m) and test (b, d, f, h, l, n) data sets. Solid lines are regression lines and dashed lines are 1:1 lines. (a, b) Equation 1 [Helz and Thornber, 1987]; (c, d) Equation 2 [Montierth et al., 1995]; (e,f) Equation 3 [Beattie, 1993]; (g,h) Equation 4 [Putirka, 2008]; (i, l) Equation 5 [Putirka, 2008]; (m, n) Equation 6 [Putirka, 2008]. Both data sets are liquids saturated with olivine ± other phases and are identical to those as in Figure 2.

| Thermometer | Calibration dataset | | | | Test dataset | | | |
|---|---|---|---|---|---|---|---|---|
| | $R^2$ | SEE (°C) | $m$ | $c$ (°C) | R2 | SEE (°C) | $m$ | $c$ (°C) |
| H&T[a], eq. 1 | 0.89 | 33 | 0.91 | 121 | 0.89 | 35 | 0.90 | 135 |
| Montierth[b], eq. 2 | 0.89 | 30 | 0.80 | 240 | 0.89 | 33 | 0.79 | 252 |
| Beattie (1993), eq. 3 | 0.92 | 21 | 0.95 | 56 | 0.91 | 24 | 0.94 | 77 |
| Putirka (2008), eq. 4 | 0.89 | 39 | 0.70 | 353 | 0.89 | 43 | 0.69 | 365 |
| Putirka (2008), eq. 5 | 0.84 | 42 | 0.74 | 297 | 0.87 | 73 | 0.74 | 292 |
| Putirka (2008), eq. 6 | 0.87 | 28 | 0.93 | 81 | 0.88 | 28 | 0.92 | 89 |
| This study, eq. 8 | 0.91 | 23 | 1 | $4 \times 10^{-10}$ | 0.90 | 25 | 0.99 | 12.4 |

[a]Helz and Thornber, [1987]. [b]Montierth et al., [1995]. Equation numbers are referenced to this study. Variables: $R^2$ – coefficient of determination; SEE – standard error of estimate; $m$, $c$ – slope and the intercept of the line fitted to the calculated vs. measured data; taking calculated data as independent variable ($x$ axis).

**Table 2.** Summary of the tested geothermometers.

The model of Putirka [2008], i.e., the eq. (4), yields $R^2 = 0.89$ and SEE = $\pm 39°$ C. When applied to the test data, the eq. (4) yields again very similar values with $R^2 = 0.89$ and SEE = $\pm 43°$ C. However, the slopes and the intercepts of the regression lines are worst, being 0.70 and 353° C for the calibration data and 0.69 and 365° C for the test data (Figure 3).

A similar result is obtained for the model of Putirka [2008], i.e., the eq. (5), with $R^2 = 0.84$ and SEE = $\pm 42°$ C for the calibration, and SEE = $\pm 43°$ C and $R^2 = 0.87$ for the test data sets, and with the slope and the intercept of the regression line 0.74 and 297° C for the calibration, and 0.74 and 292° C for the test data sets, respectively (Figure 3).

From all tested thermometers, the model of Putirka [2008], i.e., the eq. (6), similarly to the model of Beattie [1993], yields a good result when recovering $T$ for the calibration ($R^2 = 0.87$, SEE = $\pm 28°$ C) and for the test ($R^2 = 0.88$, SEE = $\pm 28°$ C) data sets. However slope and intercept of the regression lines are still poor being 0.93 and 81° C for the calibration data, and 0.92 and 89° C for the test data (Figure 3).

In summary, the eq. (3) appears to predict $T$ for both calibration and test data with an error in the range of 21-24° C, and over 1200° C it tends to slightly underestimate predicted $T$, whereas it slightly overestimates $T$ below 1200° C (Figure 3). Temperature estimates by the eq. (1) and (2) are less precise, with SEE between 33-35° C and 30-33° C, respectively. Predictions of temperature by the eq. (1) are underestimated over 1400° C and overestimated below 1400° C, those predicted by the eq. (2) are underestimated above 1200° C and overestimated below 1200° C (Figure 3). The errors of $T$ predicted by the eq. (4-5) are in the range of 39-43° C and these equations tend to underestimate the temperatures above 1175° C and above 1125° C for the eq. (4) and (5), respectively (Figure 3). In addition (Figure 3), predicted $T$ are overestimated below 1175° C by the eq. (4) and below 1125° C by the eq. (5). The equation (6) tends to overestimate the temperatures below 1120° C and to underestimate the temperatures above 1120° C with a SEE of $\pm 28°$ C (Figure 3).

Despite the eq. (1-6) are able to capture a great fraction (84-92%) of the experimental temperature variation with relatively low standard errors in the range of 21-43° C, they are affected by strong systematic errors as shown by the slopes and the intercepts of the regression lines of measured vs. calculated temperatures (Figure 3). Their lower performance, compared to that offered by the new proposed equation (8), can be explained by the following reasons: (i) the eq. (1-2) proposed by Helz and Thornber [1987] and Montierth et al. [1995] are calibrated on very specific bulk rock compositions from Hawaiian volcanoes, i.e., Kilauea lavas for eq. (1) and Mauna Loa lavas for eq. (2). Consequently, when used to predict temperatures of rocks outside their compositional calibration range, their performance decrease. However, these thermometers are by far superior with respect to

any general thermometer when applied to their specific rock composition; (*ii*) the eq. (3) proposed by Beattie [1993] and the eq. (4-6) derived by Putirka [2008] are general thermometers developed with the aim to predict temperatures for the liquids in equilibrium with olivine in a broader compositional and *P-T* range. Their low performance can be explained by their application to an anhydrous database of experiments performed solely at 1-atm with a narrower compositional range. Also, their original calibration dataset included many data points representing simplified model systems lacking some of the main chemical components. In order to avoid fitting bias (for details, see the section on Methods) these data points were excluded from our database which could have influenced the result of the regression. In summary, the eq. (8) seems to be a useful predictive tool for estimating the temperature of anhydrous silicate liquids, especially in the compositional range of basalts to andesites in equilibrium with olivine (±other phases) at one atmosphere.

### 5.3 Applications

The proposed new eq. (8) can be used as a geothermometer in particular for basalt, basaltic andesite, and andesite rocks erupted at 1-atm and temperatures in the range of 1100-1250° C. For this purpose, the eq. (8) represents a useful alternative to the other geothermometers being characterized by a lower systematic error. Temperature measurements of the Alae and Makaopuhi lava lakes, Hawaii, cover the range of 1140-1190° C [Peck, 1978; Wright and Okamura, 1977; Wright and Peck, 1978]. A comparison of these temperatures may be done with the temperatures predicted *via* different geothermometers. Apart from our equation, we choose to apply this comparison to the eq. (1-2) given they were designed specifically for the Hawaiian volcanoes [Helz and Thornber, 1987; Montierth et al., 1995], to the eq. (3) as it can be widely applied given it is based on activity-composition relations that tend to provide better extrapolations [Beattie, 1993], and to the eq. (4) given it is similar to eq. (1-2) but its calibration is based on a wider compositional range [Putirka 2008],

Using eq. (1-4) and eq. (8) in combination with the glass compositions representative of six different Hawaiian volcanoes [Garcia et al., 1989] we derive predicted temperatures which range from 1120 to 1195° C (Figure 4, 23). In particular, the eq. (8) predicts temperatures in the range of 1145-1186° C which deviate less than 15° C compared to the temperatures predicted by the equations of Beattie [1993], Montierth et al. [1995], and Putirka [2008]. Higher differences (17-25° C) between the temperatures predicted by the eq. (8) and those predicted by the equation of Helz and Thornber [1987] are ascribed to the wider compositional database that has been used to calibrate our model. Also, we note (Table 3) that one glass composition from Mauna Loa gives an unrealistic temperature of 1308° C when calculated by the model of Beattie [1993], whereas it is consistently in the range of 1166-1171° C when estimated by our equation and by the models of Montierth et al. [1995] and Putirka [2008]. The reason for this discrepancy is unclear.

Further, we employed the eq. (8) to calculate the temperatures of Atlantic MORB glassy rocks [Schilling et al., 1983] and we compared the results with the temperatures calculated by the model of Beattie [1993], i.e., the eq. (3), (Figure 4, Table 3). Differences between the results of the two models are again lower than 15° C. The comparison with a thermometer of general application, such as that of Beattie [1993], thus demonstrates the validity of our model for predicting temperatures of 1-atm magmatic systems.

## 6. Conclusions

Our understanding of how a low pressure (1-atm) magmatic system, such as a lava flow or a lava lake, might look like, and how it might evolve, hinges on our interpretation of temperatures at which the magma body stagnates and partially crystallizes. Silicate liquids in equilibrium with mineral phases provide an archive of these *T* conditions and hence the calculation of the temperature is crucial for deciphering the evolution of such magmatic systems. For a robust geothermometer, however, it is fundamental: (*i*) to be based on a large data set in order to ensure applicability to a wide range of liquid compositions; (*ii*) to be accompanied by the error estimates of both temperature recovery and prediction based on the calibration and testing (i.e., not used in the calibration process) data sets, respectively; (*iii*) to be evaluated using a regression of the observed/measured temperatures (dependent variable, *y*-axis) *vs*. predicted/calculated temperatures (independent variable, *x*-axis).
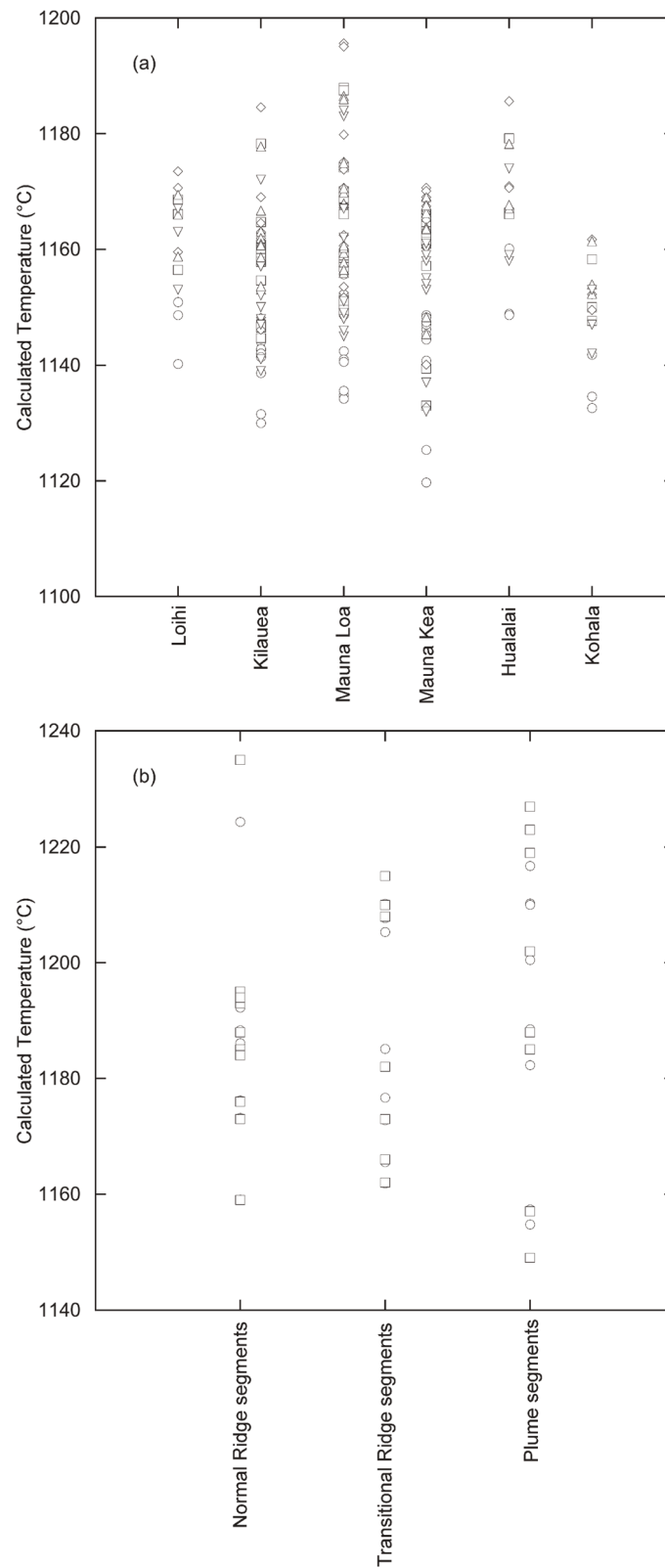
**Figure 4.** Calculated temperature for glassy samples from Hawaiian volcanoes (a) and the Mid-Atlantic Ridge (b). In panel (a) circles are temperatures calculated by eq. (1), Helz and Thornber [1987]; squares are temperatures calculated by eq. (2), Montierth et al. [1995]; downward triangles are temperatures calculated by eq. (3), Beattie [1993]; diamonds are temperatures calculated by eq. (4), Putirka [2008]; upward triangles are temperatures calculated by eq. (8), this study. In panel (b) squares are temperatures calculated by eq. (3), Beattie [1993]; circles are temperatures calculated by eq. (8), this study.

| | T (°C)[a] | T (°C)[b]/ΔT[c] | T (°C)[d]/ΔT[e] | T (°C)[f]/ΔT[g] | T (°C)[h]/ΔT[i] |
|---|---|---|---|---|---|
| Hawaiian volcanoes[l] | | | | | |
| Loihi | 1169 | 1167/2 | 1151/18 | 1169/0 | 1174/-5 |
| Loihi | 1166 | 1163/3 | 1149/17 | 1166/0 | 1171/-5 |
| Loihi | 1159 | 1153/6 | 1140/19 | 1156/3 | 1160/-1 |
| Kilauea | 1161 | 1150/11 | 1143/18 | 1159/2 | 1163/-2 |
| Kilauea | 1163 | 1152/11 | 1144/19 | 1161/2 | 1165/-2 |
| Kilauea | 1162 | 1150/12 | 1143/19 | 1159/3 | 1163/-1 |
| Kilauea | 1159 | 1147/12 | 1139/20 | 1155/4 | 1157/2 |
| Kilauea | 1178 | 1172/6 | 1159/19 | 1178/0 | 1185/-7 |
| Kilauea | 1161 | 1148/13 | 1142/19 | 1159/2 | 1162/-1 |
| Kilauea | 1161 | 1147/14 | 1141/20 | 1158/3 | 1161/0 |
| Kilauea | 1167 | 1157/10 | 1147/20 | 1165/2 | 1169/-2 |
| Kilauea | 1153 | 1139/14 | 1130/23 | 1145/8 | 1146/7 |
| Kilauea | 1154 | 1141/13 | 1132/22 | 1147/7 | 1148/6 |
| Mauna Loa | 1175 | 1167/8 | 1156/19 | 1174/1 | 1180/-5 |
| Mauna Loa | 1170 | 1162/8 | 1151/19 | 1169/1 | 1174/-4 |
| Mauna Loa | 1158 | 1148/10 | 1135/23 | 1150/8 | 1152/6 |
| Mauna Loa | 1159 | 1145/15 | 1142/17 | 1159/0 | 1162/-3 |
| Mauna Loa | 1168 | 1308/-141 | 1149/19 | 1166/2 | 1171/-3 |
| Mauna Loa | 1160 | 1151/10 | 1141/19 | 1157/3 | 1161/-1 |
| Mauna Loa | 1171 | 1162/8 | 1152/19 | 1170/1 | 1175/-4 |
| Mauna Loa | 1186 | 1183/3 | 1168/18 | 1188/-2 | 1196/-10 |
| Mauna Loa | 1161 | 1149/12 | 1141/20 | 1157/4 | 1160/-1 |
| Mauna Loa | 1156 | 1145/11 | 1134/22 | 1150/6 | 1152/4 |
| Mauna Loa | 1186 | 1184/2 | 1167/19 | 1187/-1 | 1195/-9 |
| Mauna Loa | 1156 | 1146/10 | 1136/20 | 1151/5 | 1154/2 |
| Mauna Kea | 1167 | 1160/7 | 1146/21 | 1163/4 | 1167/0 |
| Mauna Kea | 1145 | 1132/13 | 1120/25 | 1133/12 | 1133/12 |
| Mauna Kea | 1169 | 1161/8 | 1149/20 | 1166/3 | 1171/-2 |
| Mauna Kea | 1161 | 1153/8 | 1141/20 | 1157/4 | 1160/1 |
| Mauna Kea | 1167 | 1158/9 | 1147/20 | 1164/3 | 1169/-2 |
| Mauna Kea | 1148 | 1137/12 | 1125/23 | 1139/9 | 1140/8 |
| Mauna Kea | 1166 | 1158/8 | 1147/19 | 1165/1 | 1169/-3 |
| Mauna Kea | 1164 | 1155/8 | 1145/19 | 1162/2 | 1166/-2 |
| Mauna Kea | 1163 | 1154/9 | 1144/19 | 1161/2 | 1165/-2 |
| Mauna Kea | 1168 | 1159/9 | 1148/20 | 1166/5 | 1170/-2 |
| Hualalai | 1167 | 1158/7 | 1149/18 | 1166/1 | 1171/-4 |
| Hualalai | 1178 | 1174/4 | 1160/18 | 1179/-1 | 1186/-8 |
| Hualalai | 1168 | 1159/9 | 1149/19 | 1166/2 | 1171/-3 |
| Kohala | 1161 | 1153/9 | 1142/20 | 1158/3 | 1162/-1 |
| Kohala | 1154 | 1147/7 | 1133/21 | 1148/6 | 1150/-4 |
| Kohala | 1152 | 1142/10 | 1135/18 | 1150/2 | 1152/0 |
| | T (°C)[a] | T (°C)[b]/ΔT[c] | | | |
| MORB[m] | | | | | |
| Normal Ridge | 1184 | 1188/-4 | | | |
| Normal Ridge | 1224 | 1235/-11 | | | |
| Normal Ridge | 1188 | 1195/-7 | | | |
| Normal Ridge | 1186 | 1185/1 | | | |
| Normal Ridge | 1184 | 1184/0 | | | |
| Normal Ridge | 1192 | 1193/-1 | | | |
| Normal Ridge | 1173 | 1173/0 | | | |
| Normal Ridge | 1194 | 1194/0 | | | |
| Normal Ridge | 1159 | 1159/0 | | | |
| Normal Ridge | 1176 | 1176/0 | | | |
| Transition Zone | 1166 | 1162/4 | | | |
| Transition Zone | 1185 | 1182/3 | | | |
| Transition Zone | 1177 | 1173/4 | | | |
| Transition Zone | 1208 | 1210/-2 | | | |
| Transition Zone | 1173 | 1173/0 | | | |
| Transition Zone | 1210 | 1215/-5 | | | |
| Transition Zone | 1162 | 1166/-4 | | | |
| Transition Zone | 1205 | 1208/-3 | | | |
| Plume | 1155 | 1149/6 | | | |
| Plume | 1189 | 1188/1 | | | |
| Plume | 1200 | 1202/-2 | | | |
| Plume | 1182 | 1185/-3 | | | |
| Plume | 1210 | 1219/-9 | | | |
| Plume | 1157 | 1157/0 | | | |
| Plume | 1217 | 1227/-10 | | | |
| Plume | 1210 | 1223/-13 | | | |

[a]Temperature calculated by eq. (8). [b]Temperature calculated by eq. (3), Beattie [1993]. [c]Temperature difference $T^a$-$T^b$. [d]Temperature calculated by eq. (1), Helz and Thornber [1987]. [e]Temperature difference $T^a$-$T^d$. [f]Temperature calculated by eq. (2), Monthiert et al., [1995]. [g]Temperature difference $T^a$-$T^f$. [h]Temperature calculated by eq. (4), Putirka [2008]. [i]Temperature difference $T^a$-$T^h$. [l]Temperatures calculated for rocks from Hawaiian volcanoes on the basis of the glass compositions reported in Garcia et al., [1989]. [m]Temperatures calculated for rocks from the Mid-Atlantic Ridge on the basis of the glass compositions reported in Schilling et al., [1983].

**Table 3.** Predicted temperatures for glassy rocks from the Hawaiian volcanoes and from the Mid-Atlantic Ridge.

Compared to prior geothermometers in which the liquid is saturated with olivine (± other phases), our eq. (8) provides a better estimate of *T*, with standard error of estimate of ±23° C for the calibration data set, and of ±25° C for the test data set. Compared to similar liquid geothermometers, eq. (8) has been tested on a relatively large data set (*n* = 140), that was not used in the calibration process. Preferably it can be used to obtain the temperature of any anhydrous silicate liquid, with composition ranging from basalt to andesite, in equilibrium with olivine (± other phases) at 1-atm. Under these conditions the predicted temperatures are characterized by a lower systematic error than those predicted by using the previous geothermometers.

# References

Arndt, N.T. (1977). Partitioning of nickel between olivine and ultrabasic and basic komatiite liquids. Carn. Inst. Wash. Year Book, 76, 553-557.

Baker, D.R. and D.H. Eggler (1987). Compositions of anhydrous and hydrous melts coexisting with plagioclase, augite, and olivine or low-Ca pyroxene from 1 atm to 8 kbar: Application to the Aleutian volcanic center of Atka. Am. Mineral., 72, 12-28.

Baker, M.B., T.L. Grove and R. Price (1994). Primitive basalts and andesites from the Mt. Shasta region, N. California: products of varying melt fraction and water content. Contrib. Mineral. Petrol., 118, 111-129.

Barclay, J. and I.S.E. Carmichael (2004). A Hornblende basalt from Western Mexico: water-saturated phase relations constrain a pressure-temperature window of eruptibility. J. Petrol., 45, 485-506.

Barr, J.A., T.L. Grove and A.H. Wilson (2009). Hydrous komatiites from Commondale, South Africa: An experimental study. Earth Planet. Sci. Lett., 284, 199-207.

Bartels, K.S., R.J. Kinzler and T.L. Grove (1991). High pressure phase relations of primitive high-alumina basalts from Medicine Lake volcano, northern California. Contrib. Mineral. Petrol., 108, 253-270.

Beattie, P. (1993). Olivine-melt and orthopyroxene-melt equilibria. Contrib. Mineral. Petrol., 115, 103-111.

Bender, J.F., F.N. Hodges and A.E. Bence (1978). Petrogenesis of basalts from the project FAMOUS area: experimental study from 0 to 15 Kbars. Earth Planet. Sci. Lett., 41, 277-302.

Cashman, K.V., M. Mangan and S. Newman (1994). Surface degassing and modifications to vesicle size distributions in active basalt flows. J. Volcanol. Geotherm. Res., 61, 45-68.

Chen, H.K., J.W. Delano and D.H. Lindsley (1982). Chemistry and Phase relations of VLT volcanic glasses from Apollo 14 and Apollo 17. Proc. Lunar Planet. Sci. Conf., 13, A171-A181.

Costa, F., S. Andreastuti, C.B. de Maisonneuve CB and J.S. Pallister (2013). Petrological insights into the storage conditions, and magmatic processes that yielded the centennial 2010 Merapi explosive eruption. J. Volcanol. Geotherm. Res., 261, 209-235.

Delano, J.W. (1977). Experimental melting relations of 63545, 76015, and 76055. Proc. Lunar Sci. Conf., 8, 2097-2123.

de Maisonneuve, C.B., M.A. Dungan, O. Bachmann and A. Burgisser (2012). Insights into shallow magma storage and crystallization at Volcan Llaima (Andean Southern Volcanic Zone, Chile). J. Volcanol. Geotherm. Res., 211-212, 76-91.

de Maisonneuve, C.B., M.A. Dungan, O. Bachmann and A. Burgisser (2013). Petrological insights into shifts in eruptive styles at Volcan Llaima (Chile). J. Petrol., 54, 393-420.

Dunn, T. and C. Sen (1994). Mineral/matrix partition coefficients for orthopyroxene, plagioclase, and olivine in basaltic to andesitic systems; A combined analytical and experimental study. Geochim. Cosmochim. Acta, 58, 717-733.

Elkins-Tanton, L.T., N. Chatterjee and T.L. Grove (2003). Experimental and petrological constraints on lunar differentiation from the Apollo 15 green picritic glasses. Meteorit. Planet. Sci., 38, 515-527.

Fram, M.S. and J. Longhi (1992). Phase equilibria of dikes associated with Proterozoic anorthosite complexes. Am.

Mineral., 77, 605-616.

Garcia, M.O., D.W. Muenow and K.E. Aggrey (1989). Major element, volatile, and stable isotope geochemistry of Hawaiian submarine tholeiitic glasses. J. Geophys. Res., 94, B8, 10525-10538.

Gee, L.L. and R.O. Sack (1988). Experimental petrology of melilite nephelinites. J. Petrol., 29, 1233-1255.

Grove, T.L. and D.W. Beaty (1980). Classification, experimental petrology and possible volcanic histories of the Apollo 11 high-K basalts. Proc. Lunar Planet. Sci. Conf., 11, 149-177.

Grove, T.L. and W.B. Bryan (1983). Fractionation of pyroxene-phyric MORB at low pressure: An experimental study. Contrib. Mineral. Petrol., 84, 293-309.

Grove, T.L., L.T. Elkins-Tanton, S.W. Parman, N. Chatterjee, O. Müntener and G.A.

Gaetani (2003). Fractional crystallization and mantle-melting controls on calc-alkaline differentiation trends. Contrib. Mineral. Petrol., 145, 515-533.

Grove, T.L., D.C. Gerlach and T.W. Sando (1982). Origin of calc-alkaline series lavas at Medicine Lake Volcano by fractionation, assimilation and mixing. Contrib. Mineral. Petrol., 80, 160-182.

Grove, T.L. and T.C. Juster (1989). Experimental investigations of low-Ca pyroxene stability and olivine-pyroxene-liquid equilibria at 1-atm in natural basaltic and andesitic liquids. Contrib. Mineral. Petrol., 103, 287-305.

Grove, T.L., R.J. Kinzler and W.B. Bryan (1992). Fractionation of Mid-Ocean Ridge Basalt (MORB), in Melt Generation at Mid-Ocean Ridges J.P. Morgan, D.K. Blackman and J.M. Sinton JM (Editors), AGU, Washington DC, 281-310.

Helz, R.T. (1993). Thermal efficiency of lava tubes at Kilauea volcano, Hawaii, in Ancient Volcanism and Modern Analogues, IAVCEI abstracts, Canberra, 47.

Helz, R.T. and C.R. Thornber (1987). Geothermometry of Kilauea Iki lava lake, Hawaii. Bull. Volcanol., 49, 651-668.

Helz, R.T., C. Heliker, M. Mangan, K. Hon, C.A. Neal and L. Simmons (1991). Thermal history of the current Kilauean east rift eruption, Program and Abstracts: Eos, Transac., Am. Geophys. Union, sup., 72, 44, 557-558.

Helz, R.T., N.G. Banks, C. Heliker, C.A. Neal and E.W. Wolfe (1995). Comparative geothermometry and thermal history of recent Hawaiian eruptions. J. Geophys. Res., 100, 17637-17657.

Herd, C.D.K., R.E. Dwarzski and C.K. Shearer (2009). The behavior of Co and Ni in olivine in planetary basalts: An experimental investigation. Am. Mineral. 94, 244-255.

Ishibashi, H. and H. Sato (2007). Viscosity measurements of subliquidus magmas: Alkali olivine basalt from the Higashi-Matsuura district, Southwest Japan. J. Volcanol. Geotherm. Res., 160, 223-238.

Jurewicz, A.J.G., D.W. Mittlefehldt and J.H. Jones (1993). Experimental partial melting of the Allende (CV) and Murchison (CM) chondrites and the origin of asteroidal basalts. Geochim. Cosmochim. Acta, 57, 2123-2139.

Juster, T.C., T.L. Grove and M.R. Perfit (1989). Experimental constraints on the generation of FeTi basalts, andesites, and rhyodacites at the Galapagos Spreading Center, 85°W and 95°W. J. Geophys. Res., 94, 9251-9274.

Kennedy, A.K., T.L. Grove and R.W. Johnson (1990). Experimental and major element constraints on the evolution of lavas from Lihir Island, Papua New Guinea. Contrib. Mineral. Petrol., 104, 722-734.

Kenney, J. and E. Keeping (1962). Mathematics of Statistics. Volume 1, 3rd edition, Van Nostrand Company, Princeton.

Kinzler, R.J. and T.L. Grove (1985). Crystallization and differentiation of Archean komatiite lavas from northeast Ontario: phase equilibrium and kinetic studies. Am. Mineral., 70, 40-51.

Longhi, J. and V. Pan (1988). A reconnaissance study of phase boundaries in low-alkali basaltic liquids. J. Petrol., 29, 115-147.

Longhi, J., D. Walker and J.F. Hays (1978). The distribution of Fe and Mg between olivine and lunar basaltic liquids. Geochim. Cosmochim. Acta, 42, 1545-1558.

Mahood, G.A. and D.R. Baker (1986). Experimental constraints on depths of fractionation of mildly alkali basalts and associated felsic rocks: Pantelleria, Strait of Sicily. Contrib. Mineral. Petrol., 93, 251-264.

Matzen, A.K., M.B. Baker, J.R. Beckett and E.M. Stolper (2011). Fe-Mg Partitioning between Olivine and high-magnesian melts and the nature of Hawaiian parental liquids. J. Petrol., 52, 1243-1263.

Matzen, A.K., M.B. Baker, J.R. Beckett and E.M. Stolper (2013). The temperature and pressure dependence of Nickel partitioning between Olivine and silicate melt. J. Petrol., 54, 2521-2545.

Matzen, A.K., M.B. Baker, J.R. Beckett, B.J. Wood and E.M. Stolper (2017). The effect of liquid composition on the partitioning of Ni between olivine and silicate melt. Contrib. Mineral. Petrol. https://doi.org/10.1007/s00410-016-1319-8.

McCoy, T.J. and G.E. Lofgren (1999). Crystallization of the Zagami shergottite: an experimental study. Earth Planet. Sci. Lett., 173, 397-411.

Médard, E. and T.L. Grove (2008). The effect of $H_2O$ on the olivine liquidus of basaltic melts: experiments and thermodynamic models. Contrib. Mineral. Petrol., 155, 417-432.

Médard, E., M.W. Schmidt and P. Schiano (2004). Liquidus surfaces of ultracalcic primitive melts: formation conditions and sources. Contrib. Mineral. Petrol., 148, 201-215.

Meen, J.K. (1987). Formation of shoshonites from calcalkaline basalt magmas: geochemical and experimental constraints from the type locality. Contrib. Mineral. Petrol., 97, 333-351.

Meen, J.K. (1990). Elevation of potassium content of basaltic magma by fractional crystallization: the effect of pressure. Contrib. Mineral. Petrol., 104, 309-331.

Monders, A.G., E. Médard and T.L. Grove (2007). Phase equilibrium investigations of the Adirondack class basalts from the Gusev plains, Gusev crater, Mars. Meteoritic Planet. Sci. 42:131-148.

Montierth, C., A.D. Johnston and K.V. Cashman (1995). An empirical glass-composition-based geothermometer for Mauna Loa lavas, in Mauna Loa Revealed: Structure, Composition, History, and Hazards J.M. Rhodes and J.P. Lockwood (Editors), AGU, Washington DC, 207-217.

Oeser, M., P. Ruprecht and S. Weyer (2018). Combined Fe-Mg chemical and isotopic zoning in olivine constraining magma mixing-to-eruption timescales for the continental arc volcano Irazu (Costa Rica) and Cr diffusion in olivine. Am. Mineral., 103, 582-599.

Parman, S.W., J.C. Dann, T.L. Grove and M.J. de Wit (1997). Emplacement conditions of komatiite magmas from the 3.49 Ga Komati formation, Barberton Greenstone Belt, South Africa. Earth Planet. Sci. Lett., 15, 303-323.

Peck, D.L. (1978). Cooling and vesiculation of Alae lava lake, Hawaii. US Geol. Surv. Prof. Pap., 935-B.

Piñeiro, G., S. Perelman, J.P. Guerschman and J.M. Paruelo (2008). How to evaluate models: Observed vs. predicted or predicted vs. observed? Ecol. Modell., 216, 316-322.

Prissel, T.C., S.W. Parman and J.W. Head (2016). Formation of the lunar highlands Mg-suite as told by spinel. Am. Mineral., 101, 1624-1635.

Putirka, K., M. Johnson, R. Kinzler, J. Longhi and D. Walker (1996). Thermobarometry of mafic igneous rocks based on clinopyroxene-liquid equilibria, 0-30 kbar. Contrib. Mineral. Petrol., 123, 92-108.

Putirka, K.D. (2008). Thermometers and barometers for volcanic systems, in Minerals, Inclusions and Volcanic Processes K.D. Putirka, F.J.Teley III (Editors), The Mineralogical Society of America, Chantilly, 61-120.

Putirka, K.D., H. Mikaelian, F. Ryerson and H. Shaw (2003). New clinopyroxene-liquid thermobarometers for mafic, evolved, and volatile-bearing lava compositions, with applications to lavas from Tibet and the Snake River Plain, Idaho. Am. Mineral., 88, 1542-1554.

Rawlings, J.O., S.G. Pantula, and A.D. Dickey (1998). Applied Regression Analysis: A Research Tool, Second Edition, Springer, New York, 17-18.

Sack, R.O., D. Walker and I.S.E. Carmichael (1987). Experimental petrology of alkali lavas: constraints on cotectics of multiple saturation in natural basic liquids. Contrib. Mineral. Petrol., 96, 1-23.

Schilling, J.-G., M. Zajac, R. Evans, K. Johnston, W. White, J.D. Devine and R. Kingsley (1983). Petrologic and geochemical variations along the mid-Atlantic ridge from 29° N to 73° N. Am. J. Sci., 283, 510-586.

Scoates, J.S., M. Lo Cascio, D. Weis and D.H. Lindsley (2006). Experimental constraints on the origin and evolution of mildly alkali basalts from the Kerguelen Archipelago, Southeast Indian Ocean. Contrib. Mineral. Petrol., 151, 582-599.

Stamper, C.C., E. Melekhova, J.D. Blundy, R.J. Arculus, M.C.S. Humphreys and R.A. Brooker (2014). Oxides phase relations of a primitive basalt from Grenada, Lesser Antilles. Contrib. Mineral. Petrol. https://doi.org/10.1007/s00410-013-0954-6

Stolper, E.M. (1977). Experimental petrology of eucritic meteorites. Geochim. Cosmochim. Acta, 41, 587-611.

Thy, P., C.E. Lesher and M.S. Fram (1998). Low pressure experimental constraints on the evolution of basaltic lavas from site 917, southeast Greenland continental margin. Proc. Ocean Drill. Prog., 152, 359-372.

Thy, P., C.E. Lesher, T.F.D. Nielsen and C.K. Brooks (2006). Experimental constraints on the Skaergaard liquid line of descent. Lithos, 92, 154-180.

Tormey, D.R., T.L. Grove and W.B. Bryan (1987). Experimental petrology of normal MORB near the Kane Fracture Zone: 22°-25° N, mid-Atlantic ridge. Contrib. Mineral. Petrol., 96, 121-139.

Vander Auwera, J. and J. Longhi (1994). Experimental study of a jotunite (hyperstene monzodiorite): constraints on the parent magma composition and crystallization conditions ($P$, $T$, $fO_2$) of the Bjerkreim-Sokndal layered intrusion (Norway). Contrib. Mineral. Petrol., 118, 60-78.

Vander Auwera, J., J. Longhi and J.C. Duchesne (1998). A liquid line of descent of the Jotunite (Hyperstene Monzodiorite) suite. J. Petrol., 39, 439-468.

Veksler, I.V., A.M. Dorfman, A.A. Borisov, R. Wirth and D.B. Dingwell (2007). Liquid immiscibility and the evolution of basaltic magma. J. Petrol., 48, 2187-2210.

Wang, Z. and G.A. Gaetani (2008). Partitioning of Ni between olivine and siliceous eclogite partial melt: experimental constraints on the mantle source of Hawaiian basalts. Contrib. Mineral. Petrol., 156, 661-678.

Wright, T.L. and D.L. Peck (1978). Crystallization and differentiation of the Alae magma, Alae lava lake, Hawaii. US Geol. Surv. Prof. Pap., 935-B.

Wright, T.L. and R.T. Okamura (1977). Cooling and crystallization of tholeiitic basalt, 1965 Makaopuhi lava lake, Hawaii. US Geol. Surv. Prof. Pap., 1004.

Yang, H.J., F.A. Frey, D.A. Clague and M.O. Garcia (1999) Mineral chemistry of submarine lavas from Hilo Ridge, Hawaii: implications for magmatic processes within Hawaiian rift zones. Contrib. Mineral. Petrol., 135, 355-372.

Zhang, Y.S., T. Hou, I.V. Veksler, C.E. Lesher and O. Namur (2018). Phase equilibria and geochemical constraints on the petrogenesis of high-Ti picrite from the Paleogene East Greenland flood basalt province. Lithos, 300, 20-32.

**\*CORRESPONDING AUTHOR: Alessandro FABBRIZIO**,
Institute of Petrology and Structural Geology, Faculty of Science,
Charles University, Albertov 6, 12843 Prague, Czech Republic;
e-mail: alessandro.fabbrizio@natur.cuni.cz,
+420221951525,